ChemComm

Cite this: *Chem. Commun.*, 2011, **47**, 6963–6965

www.rsc.org/chemcomm

COMMUNICATION

Facile preparation of SERS-active nanogap-rich Au nanoleaves†

Jin-Hyung Hong,‡[a] Yong-Kyung Hwang,‡[a] Jin-Yeon Hong,[a] Hee-Jin Kim,[b] Sung-Jin Kim,[b] Yong Sun Won[c] and Seong Huh*[a]

Received 17th March 2011, Accepted 28th April 2011
DOI: 10.1039/c1cc11539a

To simply reduce $HAuCl_4$ using 2-thiophenemethanol in an aqueous solution at room temperature, a novel metallic Au nanostructure with a high SERS activity was obtained. Flat sheet-like Au nanoleaves possessing many nanogap hotspots bound with a large percentage of high-index facets were obtained.

Nanostructured metallic Au attracts much attention in a variety of fields such as optical sensors,[1] surface-enhanced Raman scattering (SERS) active surface,[2] catalysis,[3] and intracellular gene and drug delivery systems.[4] A wide range of different particle shapes has been reported in the literature.[5] Triangular prisms and thin hexagonal plate nanoscale Au were also reported.[6] They are suited for optical sensors due to the plasmon-enhanced optical absorptions.[7] Several reports mentioned the preparation of gold nanosheets.[8] Most of them were obtained under chemical reduction conditions. In this case, however, shape control was primarily achieved by extra organic capping ligands on the surfaces of the metallic nanosheets. In general, a narrow range of synthetic conditions is required to obtain the desired morphology.

Herein, we describe a novel seedless synthetic approach to prepare a nanogap-rich Au nanoleaf structure in an aqueous solution at room temperature. 2-Thiophenemethanol was chosen as a reducing agent for the reduction of a trivalent Au precursor to metallic Au because the standard reduction potential of $AuCl_4^- + 3e^- \rightarrow Au(s) + 4Cl^-$ is 1.002 V at STP and the formal reduction potential of 2-thiophenemethanol in phosphate buffered saline (PBS, pH 7.0) estimated from cyclic voltammetry is 0.76 V (Fig. S1, ESI†). No additional organic capping ligands were used in our synthetic conditions. 2-Thiophenemethanol may either dimerize into 5,5′-dihydroxymethyl-2,2′-bithiophene or oligomerize to various oligomers through an oxidative coupling during the redox reaction as shown in Scheme 1.

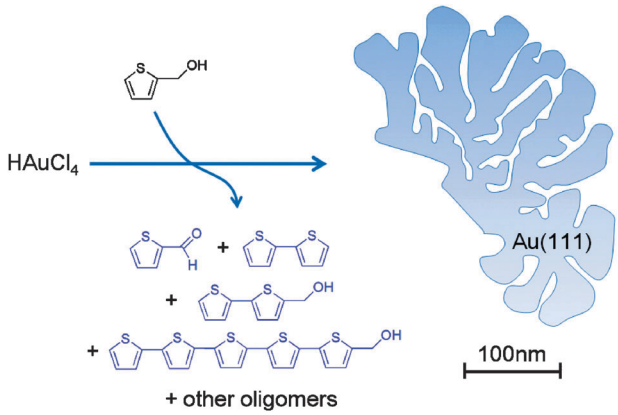

Scheme 1 The proposed formation pathway of the nanogap-rich Au nanoleaves in the presence of 2-thiophenemethanol as a reducing agent. The *in situ* generated thiophene derivatives stabilize Au surfaces.

We envisioned that oligomerized 2-thiophenemethanol might also behave as structure-directing capping ligands to give rise to novel morphology of nanostructured metallic Au.

In a typical example of synthesis, 2-thiophenemethanol (0.106 mmol, 10 μL) dissolved in 10 mL of distilled water was vigorously stirred for about 1 min. Then, $HAuCl_4 \cdot 3H_2O$ (0.102 mmol, 40 mg) was added to the solution. The resulting solution was gently stirred at 60 rpm for 6 h at room temperature. The suspension was centrifuged at 9000 rpm for 20 min, and the precipitates were collected and washed with distilled water several times, and finally redispersed in 10 mL of distilled water. In order to elucidate the shape control efficiency of 2-thiophenemethanol, we also gradually varied the relative molar ratio of the gold precursor and 2-thiophenemethanol: the Au/S molar ratio for GN1 = 1 : 0.52, GN2 = 1 : 1.04, and GN3 = 1 : 2.08, where GN stands for gold nanoleaf.

The final products were characterized by transmission electron microscopy (TEM) and scanning electron microscopy (SEM). TEM and SEM images of GN1, GN2, and GN3 samples are shown in Fig. 1. Interestingly, all three samples exhibit similar nanoleaf morphology. They show a very complicated yet overall a consistent pattern which was not previously observed for nanostructured gold materials. Although the detailed shape formation mechanism is not clearly understood now, the 2-thiophenemethanol together with its oxidatively coupled dimer or oligomers might behave as shape controlling capping ligands

[a] *Department of Chemistry and Protein Research Center for Bio-Industry, Hankuk University of Foreign Studies, Yongin 449-791, Korea. E-mail: shuh@hufs.ac.kr; Fax: +82 31 3304566; Tel: +82 31 3304522*
[b] *Department of Chemistry and Nano Science, Ewha Womans University, 11-1 Daehyun-dong, Seodaemun-gu, Seoul 120-750, Korea*
[c] *Department of Chemical Engineering, Pukyong National University, Pusan 608-739, Korea*

† Electronic supplementary information (ESI) available: Experimental details, HRTEM images and EDS analysis result, UV/Vis spectrum, mass spectrometry analysis data, XPS, and Raman spectra. See DOI: 10.1039/c1cc11539a

‡ These authors contributed equally.

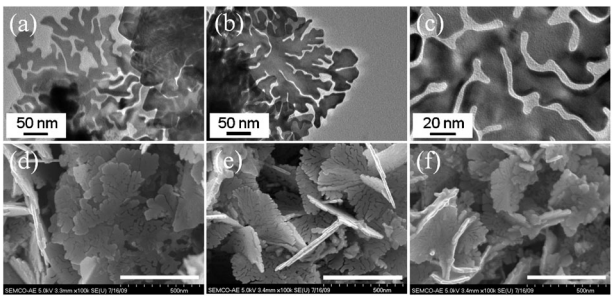

Fig. 1 TEM images of Au nanoleaves (a) GN1, (b) GN2, and (c) GN3. SEM images of the corresponding Au nanoleaves (d) GN1, (e) GN2, and (f) GN3. Scale bars for SEM images are 500 nm.

to induce an anisotropic growth of the Au nanostructure. Despite the complex structure of Au nanoleaves, the single nanoleaf maintains constant thickness for the entire area as evidenced by the SEM side view in Fig. 1e. The measured thicknesses of the samples are in the range of 7–18 nm (Fig. S2, ESI†). These values are comparable to those of Au nanosheets that appeared in the literature.[8] Energy-dispersive X-ray spectroscopy (EDS) analysis confirmed the composition of the pure Au nanoleaves as shown in Fig. S3 (ESI†).

The variation of the molar ratio of the Au precursor to 2-thiophenemethanol did not significantly alter the overall morphology of the Au nanoleaves as shown in Fig. 1.

The TEM study of GN3 indicated that the top and bottom surfaces of nanoleaves are exclusively bound with {111} facets of the face-centered cubic (fcc) Au lattice (Fig. 2c). The observed selected area electron diffraction (SAED) pattern was a hexagonal symmetry spot pattern (Fig. 2d). The SAED pattern exhibited 1/3{422}, {220}, and {311} Bragg reflections which implies that GN3 has atomically flat single crystalline geometry.[6c] The lattice fringe of 2.35 Å correspnding to the (111) plane of fcc Au was also confirmed (Fig. S4, ESI†).[9] We often observed very nice Moiré fringes on stacked nanoleaves (Fig. S5, ESI†). We measured the gap dimensions in a Au nanoleaf using arbitrarily chosen 120 lines as depicted in Fig. 2a. The average dimension of nanogaps is around 4.38 nm (Fig. 2b). Also most of the nanogap dimensions are smaller than 10 nm. This range of nanogap dimensions is suited for the generation of so-called hotspots in SERS.[10]

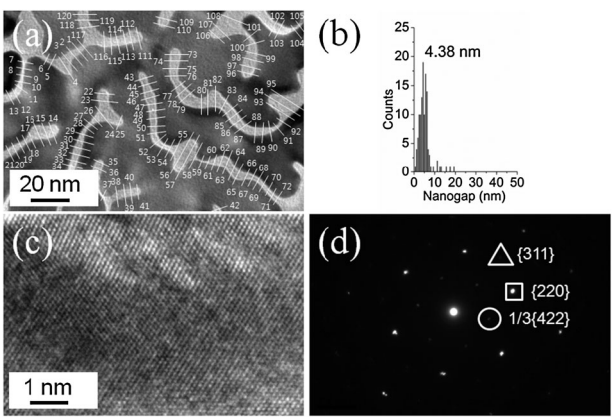

Fig. 2 (a) TEM image of Au nanoleaf, GN3. The numbers and lines indicate the basis sets for nanogap dimension measurements. (b) Distribution of nanogap dimensions based on the lines indicated in (a). (c) HRTEM image of the flat top face indicating the hexagonally symmetric {220} plane of fcc Au. (d) The SAED pattern of the top surface of GN3. A weak formally forbidden 1/3{422} reflection is also visible.

Powder X-ray diffraction (PXRD) patterns also revealed the single crystalline nature of the fcc Au nanoleaves. Five well resolved diffraction peaks from the (111), (200), (220), (311), and (222) diffraction planes of fcc Au were observed as shown in Fig. 3. The intensity ratio of (200) to (111) diffraction peaks, I_{200}/I_{111}, is 0.38 which is lower than the known standard value of 0.51 from JCPDS No. 04-0784. However, all other intensity ratios, I_{220}/I_{111} (= 0.51), I_{311}/I_{111} (= 0.48), and I_{222}/I_{111} (= 0.22), exhibit larger values than the corresponding values of bulk Au: 0.32, 0.36, and 0.12, respectively. Since the geometry of a single crystalline Au nanoleaf is flat and the basal planes are bound with {111} facets, the high-index facets, {220}, {311}, and {222}, must cover the surfaces of nanogap edges. The high-resolution TEM (HRTEM) image of the nanogap revealed the existence of high-index facets, {220} and {311}, as shown in Fig. S6 (ESI†). Lattice spacings of 2.35 Å and 2.05 Å were observed along the [011] zone axis and they correspond to {111} and {200} facets, respectively.[9] One may speculate that it is the *in situ* generated sulfur-containing thiophene derivatives that play a significant role of unusual surface growth and passivation.

UV/Vis spectra obtained during the formation of Au nanoleaves, GN3, are shown in Fig. S7 (ESI†). At the beginning stage, a weak broad surface plasmon resonance (SPR) band centered at around 595 nm became dominant until 20 min (Fig. S7a, ESI†). This SPR band may be attributed to the coexistence of nanoparticles and tiny thin sheet-like particles. Generally, uniform spherical Au nanoparticles exhibit a sharp SPR band at 520 nm and the band maxima move to higher values with increasing size of nanoparticles.[11] As the reaction progressed, however, this SPR band gradually disappeared (Fig. S7b, ESI†). After 2 h of reaction, no discernible SPR band was observed in the same wavelength region. To probe the reaction mechanism, we analyzed the reaction mixture periodically by TEM (Fig. S8, ESI†). Only small Au nanoparticles embedded in 2-thiophenemethanol oligomers were observed at 20 min. After 150 min, however, well developed Au nanoleaves are dominant species. The nanogap formation may be attributed to the residual 2-thiophenemethanol oligomers

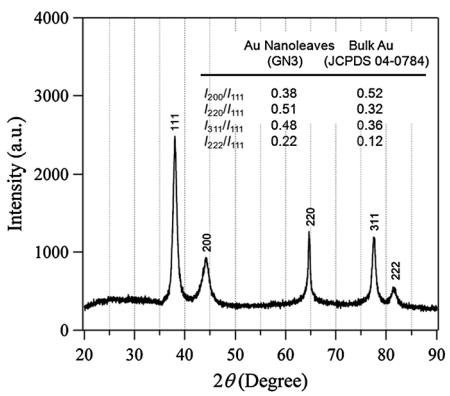

Fig. 3 PXRD pattern of Au nanoleaves, GN3.

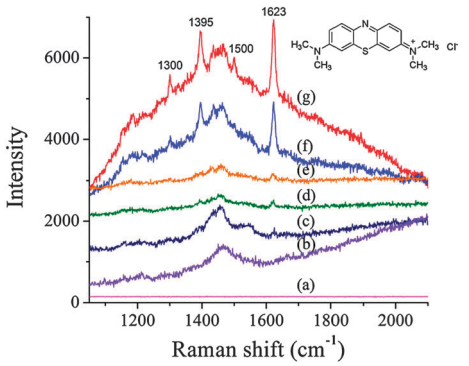

Fig. 4 Concentration-dependent Raman spectra of (a) the MB solution (1×10^{-5} M) on a flat Au coated glass, (b) the supernatant of the reaction mixture without MB treatment, and MB solutions on GN3 samples on a Si wafer (c) 1×10^{-9} M, (d) 1×10^{-8} M, (e) 1×10^{-7} M, (f) 1×10^{-6} M, and (g) 1×10^{-5} M. The chemical structure of MB is drawn together.

which selectively block the certain lateral growth directions of Au nanoleaves.

The formation of various 2-thiophenemethanol derivatives was confirmed from ESI mass spectrometry analysis of the reaction mixture (Fig. S9, ESI†). There are various species derived from 2-thiophenemethanol as well as a simple oxidized product, 2-thiophenecarboxaldehyde. Therefore, the oxidation might occur through both the oxidative coupling of 2-thiophenemethanol and oxidation of the hydroxymethyl group of 2-thiophenemethanol.

X-Ray photoelectron spectroscopy (XPS) revealed the state of Au atoms in GN samples. Au 4f peaks found at 87.32 eV ($4f_{5/2}$) and 83.57 eV ($4f_{7/2}$) confirmed the zero-valent metallic Au state (Fig. S10, ESI†).[12] In addition, there are S 2s, S 2p, C 1s, and O 1s peaks and this indicates that the oligomerized sulfur-containing thiophenemethanol derivatives are adsorbed on the surface of Au nanoleaves because of the strong tendency of a S atom to the Au surface (Fig. S11, ESI†). They may play a key role in inducing the flat geometry with a (111) plane-rich thin sheet-like Au structure by selective passivation of the (111) plane. We speculate that the sulfur-contaning organic species are also responsible for the nanogap formation. Once 2-thiophenemethanol was replaced by 3-thiophenemethanol under the same reaction conditions, a quite different product was obtained. The latter can polymerize to form high molecular weight polythiophenes due to the free 2- and 5-positions. The TEM image of the product showed small monodispersed Au nanoparticles completely surrounded by the polythiophene conducting polymer matrix (Fig. S12, ESI†).

The presence of a nanometre range of gaps will induce an enhanced localized electric field for an efficient Raman signal enhancement for analytes located in the gaps. To verify the Raman signal enhancements, GN3 was spin-coated on a Si wafer and varying concentrations of aqueous methylene blue (MB) solutions were treated on the substrate. MB has a characteristic Raman signal at 1623 cm^{-1}.[13] The peak intensity was compared with that of pure MB on a control flat Au coated microscope slide glass purchased from Aldrich (layer thickness 100 Å, catalog no. 643203). As expected, no signals were detected for the highest concentration sample of 10^{-5} M MB solution with an increased laser power of 1 mW as in Fig. 4a. While very broad signals observed between 1400 and 1600 cm^{-1} for the reaction supernatant in Fig. 4b can be attributed to the surface adsorbed thiophene derivatives. On the other hand, GN3 treated with 10^{-5} M MB solution clearly showed an intense signal at 1623 cm^{-1} (Fig. 4g). Different concentrations of MB solutions were tested to estimate the detection limit using the GN3 (Fig. 4c–f). Surprisingly, we could observe the characteristic Raman signal of MB up to 10^{-9} M concentration (Fig. 4c). The enhancement factor (EF) was estimated to be $\sim 2.0 \times 10^8$ (Fig. S13, ESI†). The SERS intensity is quite reliable. We undertook another SERS experiment using crystal violet (CV) with varying concentrations (Fig. S14, ESI†). The characteristic CV signal at 1617 cm^{-1} was also successfully detected up to 10^{-8} M concentration. However, we did not observe any signal enhancement with an excitation at 514 nm (Fig. S15, ESI†).

In summary, the use of 2-thiophenemethanol as a reducing agent for the preparation of nanoscale Au materials is an efficient method to obtain anisotropically grown Au nanosheets with an unprecedented structural motif and superb SERS activity. The high EF can be attributed to the well-developed nanogap hotspots which are evenly distributed in the Au nanoleaves. We envision that the nanogap-rich Au nanoleaves would be applicable to many useful applications.

This work was supported by the Gyeonggi Regional Research Center (GRRC) program of Gyeonggi province (GRRC-HUFS-2010-A01).

Notes and references

1 (*a*) C. A. Mirkin, R. L. Letsinger, R. C. Mucic and J. J. Storhoff, *Nature*, 1996, **382**, 607; (*b*) Q. Zheng, C. Han and H. Li, *Chem. Commun*., 2010, **46**, 7337.
2 (*a*) R. S. Golightly, W. E. Doering and M. J. Natan, *ACS Nano*, 2009, **3**, 2859; (*b*) D. Graham, *Angew. Chem., Int. Ed*., 2010, **49**, 9325.
3 (*a*) M. Haruta, N. Yamada, S. Iijima and T. Kobayashi, *J. Catal*., 1989, **115**, 301; (*b*) A. Corma and H. Garcia, *Chem. Soc. Rev*., 2008, **37**, 2096.
4 D. A. Giljohann, D. S. Seferos, W. L. Daniel, M. D. Massich, P. C. Patel and C. A. Mirkin, *Angew. Chem., Int. Ed*., 2010, **49**, 3280.
5 (*a*) X. Lu, H.-Y. Tuan, B. A. Korgel and Y. Xia, *Chem.–Eur. J*., 2008, **14**, 1584; (*b*) F. Kim, S. Connor, H. Song, T. Kuykendall and P. Yang, *Angew. Chem., Int. Ed*., 2004, **43**, 3673.
6 (*a*) R. Jin, Y. C. Cao, E. Hao, G. S. Métraux, G. C. Schatz and C. A. Mirkin, *Nature*, 2003, **425**, 487; (*b*) C. Xue, X. Chen, S. J. Hurst and C. A. Mirkin, *Adv. Mater*., 2007, **19**, 4071; (*c*) S. S. Shankar, A. Rai, B. Ankamwar, A. Singh, A. Ahmad and M. Sastry, *Nat. Mater*., 2004, **3**, 482.
7 (*a*) Y. Shen, M. Kuang, Z. Shen, J. Nieberle, H. Duan and H. Frey, *Angew. Chem., Int. Ed*., 2008, **47**, 2227; (*b*) G. Walters and I. P. Parkin, *J. Mater. Chem*., 2009, **19**, 574; (*c*) C. L. Nehl and J. H. Hafner, *J. Mater. Chem*., 2008, **18**, 2415.
8 (*a*) T. Soejima and N. Kimizuka, *Chem. Lett*., 2005, 1234; (*b*) T. Soejima and N. Kimizuka, *J. Am. Chem. Soc*., 2009, **131**, 14407.
9 J. Xu, S. Li, J. Weng, X. Wang, Z. Zhou, K. Yang, M. Liu, X. Chen, Q. Cui, M. Cao and Q. Zhang, *Adv. Funct. Mater*., 2008, **18**, 277.
10 S. Y. Lee, L. Hung, G. S. Lang, J. E. Cornett, I. D. Mayergoyz and O. Rabin, *ACS Nano*, 2010, **4**, 5763.
11 (*a*) H. Li, J. Jo, J. Wang, L. Zhang and I. Kim, *Cryst. Growth Des*., 2010, **10**, 5319; (*b*) X. Sun, S. Dong and E. Wang, *Angew. Chem., Int. Ed*., 2004, **43**, 6360.
12 K. Y. Lee, M. Kim, J. Hahn, J. S. Suh, I. Lee, K. Kim and S. W. Han, *Langmuir*, 2006, **22**, 1817.
13 D. A. Walker, K. P. Browne, B. Kowalczyk and B. A. Grzybowski, *Angew. Chem., Int. Ed*., 2010, **49**, 6760.